Engineering Analysis with Boundary Elements 34 (2010) 471–476

Contents lists available at ScienceDirect

Engineering Analysis with Boundary Elements

journal homepage: www.elsevier.com/locate/enganabound

Electrophoretic mobility of a colloidal cylinder between two parallel walls

Dustin L. House, Haoxiang Luo *

Department of Mechanical Engineering, Vanderbilt University, 2301 Vanderbilt Pl, Nashville, TN 37235-1592, USA

ARTICLE INFO

Article history:
Received 29 May 2009
Accepted 25 October 2009
Available online 29 December 2009

Keywords:
Electrokinetic transport
Electrophoresis
Electrophoretic mobility
Particle motion
Microchannel boundary effects
Microfluidics

ABSTRACT

Electrophoresis of a cylindrical particle placed between two parallel walls is considered for arbitrary eccentricity. The electric field is perpendicular to the particle axis, and both the particle and walls are non-conducting. The electrical double layers adjacent to the solid surfaces are assumed to be thin with respect to the particle radius and to the particle–wall gap. A boundary-element method is used to solve the governing equations. It is found that the viscous effect becomes comparable to the electrophoresis when the ratio between the channel width and cylinder diameter approaches unity. In addition, the eccentricity has a significant effect on the particle's rotation.

1. Introduction

The electrophoresis of colloidal particles near boundaries has been the topic of many studies due to its applications in microfluidic devices [1]. It is well known that in an unbounded flow, the electrophoretic motion of a non-conducting particle with arbitrary shape is purely translational, and the velocity can be described by Smoluchowski's formula. However, when the particle is near a wall, its mobility may change significantly due to modification of the electric field by the presence of the wall. In fact, it was found that the translational velocity of a spherical particle is increased as the particle is sufficiently close to the wall [2–4]. This result is in sharp contrast to the intuitive idea that when compared to a particle in unbounded flow, a particle traveling along a wall would be slowed down due to the increased viscous force, as seen in the Stokes mobility problem.

Electrophoretic motion of a particle near boundaries has been studied for various configurations. The translation of a spherical particle near a wall was analyzed by Keh and Chen [3] for insulating surfaces using the eigenfunction series, and their study was later complemented by Yariv and Brenner [5] for closer particle–wall separation using an asymptotic expansion. Other configurations include spheroids, cylinders, or ellipsoids in confined environments such as cylindrical pores [4,6], spherical cavities [7,8], and complex channels [9,10]. Despite these works, the electrophoretic mobility of an infinite cylindrical particle bounded by two parallel walls and translating perpendicular to its own axis has not been reported. The problem emulates the situation where a slender particle moving sideways in a microchannel. Keh et al. [11] derived an analytical solution for an infinite, insulating cylinder electrophoretically moving along a single non-conducting wall and found that the velocity grows unboundedly as the cylinder–wall separation approaches zero. It is not clear yet how the cylinder's mobility would change if it is bounded from both sides. One relevant situation to this issue is the electrophoresis of a spherical particle moving between two parallel walls, which was studied analytically by Unni et al. [12] for arbitrary eccentricity. In Unni et al., the particle's translation is found to be enhanced when both walls are close to the particle, which implies that the increasing electrophoretic effect has overcome the hydrodynamic retardation for the close particle-wall separation. However, this phenomenon may not occur in the two-dimensional case, where the closely fitting cylinder is subject to a "piston effect" and will experience much higher hydrodynamic resistance than the spherical particle in the channel. In this sense, the confined cylinder is more like the sphere in a narrow cylindrical pore, whose electrophoretic mobility decreases significantly when the particle-to-pore radius ratio approaches to unity [4].

In electrokinetic flows, a charged surface, either a wall or particle, draws counter-ions in the electrolyte toward the surface, forming a non-neutral diffuse layer covering the surface, called electrical double layer (EDL). With an externally applied electric field, the fluid in the EDL moves relative to the surface in the tangential direction, and the electric body force in the EDL is balanced by the viscous stress. When the thickness of the EDL, or Debye length, k^{-1}, is much smaller than the characteristic length scale of the surface, say, the particle radius, a, such that $ka \gg 1$, a common practice is to treat the EDL as a singular surface with zero thickness and introduce a "slip" velocity between the solid

* Corresponding author. Tel.: +1 615 322 2079; fax: +1 615 343 6687.
E-mail address: haoxiang.luo@vanderbilt.edu (H. Luo).

0955-7997/$ - see front matter © 2009 Elsevier Ltd. All rights reserved.
doi:10.1016/j.enganabound.2009.10.015

surface and the fluid in contact with it [13,2]. The slip velocity is equal to the velocity of the outer edge of the EDL and is given by the Helmholtz expression. With this thin-EDL approximation, only the electric field and the neutral fluid in the bulk region need to be dealt with, and the resulting system is governed by linear equations, more specifically, the Laplace and Stokes equations.

Analytical approaches have been used to solve the governing equations for the electrokinetic flows, for example, the reflection method [3] and the asymptotic expansion using a reciprocal theorem [5]. These approaches are restricted to problems with simple geometries and often with vanishing parameters, e.g., the ratio of the particle–wall separation to the particle size. On the other hand, numerical approaches are able to handle more complex geometries. However, the numerical methods that are based on volume discretization, such as the finite-element method (FEM) [9,6,10], have limited accuracy and are not suitable for the problems with small particle–wall separation where both the small gap and bulk region have to be resolved. The boundary element method (BEM), which requires a surface mesh only, is far superior to the FEM in accuracy and efficiency for a wide range of problems. In particular, for the thin-EDL flows where the governing equations are linear, the BEM provides an attractive approach for arbitrary geometric configurations. Indeed, the BEM has been adopted for such problems by some previous authors [14,15], but its usage is still rather limited. Therefore, this paper's purpose is two-fold. First, we will adopt the BEM to solve the aforementioned two-dimensional problem of an electrophoresis-driven particle in a channel with arbitrary eccentricity. Second, we intend to make the community aware of the BEM and freely available BEM library [16] as an alternative to the commercial FEM packages.

2. Problem specification and governing equations

We consider a cylindrical particle suspended in an aqueous electrolyte solution between two parallel walls, as shown in Fig. 1. The axis of the cylinder is parallel to the walls and is perpendicular to the uniform, external electric field, E^∞. The problem configuration is two-dimensional, where the particle may rotate about the z-axis while translating in the x direction. Both the particle and the channel walls are non-conducting and carry uniform surface charges, which are characterized by their respective zeta potentials, ζ_p and ζ_w. A positively charged surface has a positive value of zeta potential. We assume that the thickness of the EDL adjacent to the particle surface and walls is sufficiently small so that the thin-EDL approximation may be used. With the approximation, the entire flow field is neutral, and the distribution of the electric potential, ϕ, is governed by the Laplace equation,

$$\nabla^2\phi = 0, \tag{1}$$

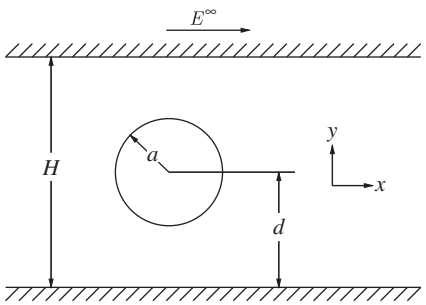

Fig. 1. Schematic of the cylindrical particle suspended in an aqueous solution between two parallel walls.

subject to the homogeneous Neumann boundary condition, $\partial\phi/\partial\mathbf{n} = 0$, at the particle surface and channel walls [5]. Note that $\mathbf{n}$ is the surface normal and points into the flow.

The fluid is Newtonian and incompressible, and the Reynolds number is small so that the fluid inertia can be ignored. The bulk flow is then governed by the Stokes and continuity equations

$$-\nabla p + \mu\nabla^2\mathbf{u} = 0, \quad \nabla\cdot\mathbf{u} = 0, \tag{2}$$

where p, $\mathbf{u} = (u_x, u_y)$, and μ are pressure, velocity, and viscosity, respectively. Under the thin-EDL assumption, the fluid velocity next to the particle or channel walls can be expressed as a slip velocity that is relative to the solid surfaces and is proportional to the local tangential gradient of the electric potential [2],

$$\mathbf{u}^S = \frac{\varepsilon\zeta}{\mu}(\mathbf{l}-\mathbf{nn})\cdot\nabla\phi, \tag{3}$$

where $\mathbf{u}^S$ is the slip velocity, ε is the dielectric constant of the electrolyte solution, $\zeta = \zeta_p$ or ζ_w is the zeta potential on either the particle surface or channel wall, and $(\mathbf{l}-\mathbf{nn})$ is the surface gradient operator. In the laboratory coordinates, the fluid velocity at the particle surface is the combination of the rigid body motion of the particle and the slip velocity,

$$\mathbf{u}(\mathbf{x}) = \mathbf{u}^B + \mathbf{u}^S = \mathbf{u}_c + \omega\mathbf{e}_z\times(\mathbf{x}-\mathbf{x}_c) + \mathbf{u}^S, \tag{4}$$

where $\mathbf{x}$ is a point on the particle surface, $\mathbf{x}_c$ and $\mathbf{u}_c$ are the position and velocity of the centroid of the particle, ω is the rotational speed of the particle, $\mathbf{e}_z$ is the unit vector in z, and $\mathbf{u}^B = \mathbf{u}_c + \omega\mathbf{e}_z\times(\mathbf{x}-\mathbf{x}_c)$ is the velocity of the point $\mathbf{x}$ due to the rigid body motion. The particle is assumed to be neutrally buoyant in the fluid, and its inertia can also be ignored. Therefore, both the total traction and torque exerted on the particle vanish,

$$\int_P \mathbf{f}\,dl = \mathbf{0}, \quad \int_P (\mathbf{x}-\mathbf{x}_c)\times\mathbf{f}\,dl = \mathbf{0}, \tag{5}$$

where $\mathbf{f} = (f_x, f_y)$ is the local traction, and the integrations are performed over the particle contour, P. At the two channel ends, which are far away from the particle, we assume that flow is fully developed so that the velocity no longer depends on x.

3. Boundary element formulation

Note that the solution of Eq. (1) is independent of the solution of Eq. (2), while the latter depends on the former through the boundary condition equation (3). Therefore, Eqs. (1) and (2) can be solved sequentially. We utilize a boundary integral method [17] to solve the governing equations.

The electric potential, ϕ, is decomposed into the combination of the background potential, $\phi^\infty = -E^\infty x$, and the disturbance potential generated due to the presence of the particle, ϕ^D, so that $\phi = \phi^\infty + \phi^D$. Following the boundary integral formulation, the disturbance potential in the interior of the flow field can be written as

$$\phi^D(\mathbf{x}_0) = -\int_C G(\mathbf{x},\mathbf{x}_0)[\mathbf{n}\cdot\nabla\phi^D]\,dl(\mathbf{x}) + \int_C \phi^D[\mathbf{n}\cdot\nabla G(\mathbf{x},\mathbf{x}_0)]\,dl(\mathbf{x}), \tag{6}$$

where $\mathbf{x} = (x, y)$, $\mathbf{n}$ is the surface normal pointing into the flow field, $r = |\mathbf{x}-\mathbf{x}_0|$, and

$$G(\mathbf{x},\mathbf{x}_0) = -\frac{1}{2\pi}\ln r, \tag{7}$$

$$\frac{\partial G}{\partial x} = -\frac{1}{2\pi}\frac{x-x_0}{r^2}, \quad \frac{\partial G}{\partial y} = -\frac{1}{2\pi}\frac{y-y_0}{r^2}, \tag{8}$$

are, respectively, the free-space Green's function of the two-dimensional Laplace equation and its associated gradient (e.g., [16]).

In Eq. (6), the integrations are performed over the particle and wall contours denoted by C. The equation is subject to the boundary conditions $\partial\phi^D/\partial\mathbf{n}=0$ on the walls, $\partial\phi^D/\partial\mathbf{n}=-\partial\phi^\infty/\partial\mathbf{n}$ on the particle surface, and $\phi^D\to 0$ as $x\to\pm\infty$. Applying (6) on either the walls or particle surface and rearranging, we have

$$-\frac{1}{2}\phi^D(\mathbf{x}_0)+\int_C \phi^D[\mathbf{n}\cdot\nabla G(\mathbf{x},\mathbf{x}_0)]\,dl(\mathbf{x})=\int_C G(\mathbf{x},\mathbf{x}_0)[\mathbf{n}\cdot\nabla\phi^D]\,dl(\mathbf{x}), \tag{9}$$

where the explicit terms containing known boundary conditions have been grouped into the right-hand side of the equation.

Similarly, we decompose the fluid velocity into the background velocity,

$$u^\infty=-\frac{\varepsilon\zeta_w E^\infty}{\mu}, \tag{10}$$

which is the uniform electroosmotic flow in the absence of the particle, and the disturbance velocity generated by the particle, $\mathbf{u}^D$, so that $\mathbf{u}^D=u^\infty\mathbf{e}_x+\mathbf{u}^D$. The disturbance velocity vanishes as x approaches infinity. To compute the disturbance velocity, we use the boundary integral formulation for Stokes flow and express $\mathbf{u}^D$ at the point $\mathbf{x}_0$ that lies inside the fluid in the following form:

$$\mathbf{u}^D(\mathbf{x}_0)=-\frac{1}{4\pi\mu}\int_C f_i^D(\mathbf{x})G_{ij}(\mathbf{x},\mathbf{x}_0)\,dl(\mathbf{x})+\frac{1}{4\pi}\int_C u_i^D(\mathbf{x})T_{ijk}(\mathbf{x},\mathbf{x}_0)n_k(\mathbf{x})\,dl(\mathbf{x}), \tag{11}$$

where C represents the particle surface and channel walls, $\mathbf{f}^D$ is the disturbance traction, and

$$G_{ij}(\mathbf{x},\mathbf{x}_0)=-\delta_{ij}\ln r+\frac{\hat{x}_i\hat{x}_j}{r^2},\quad T_{ijk}(\mathbf{x},\mathbf{x}_0)=-4\frac{\hat{x}_i\hat{x}_j\hat{x}_k}{r^4}, \tag{12}$$

are, respectively, the free-space Green's function of two-dimensional Stokes flow and associated stress tensors, $\hat{\mathbf{x}}=\mathbf{x}-\mathbf{x}_0$, and $r=|\hat{\mathbf{x}}|$ (e.g., [17]).

To simplify the integral expressions, we use $\mathcal{S}$ and $\mathcal{D}$ to represent the single- and double-layer potentials in Eq. (11), whose components are given by

$$\mathcal{S}_j(\mathbf{x}_0,\mathbf{f},C)\equiv\int_C f_i(\mathbf{x})G_{ij}(\mathbf{x},\mathbf{x}_0)\,dl(\mathbf{x}),$$

$$\mathcal{D}_j(\mathbf{x}_0,\mathbf{u},C)\equiv\int_C u_i(\mathbf{x})T_{ijk}(\mathbf{x},\mathbf{x}_0)n_k(\mathbf{x})\,dl(\mathbf{x}), \tag{13}$$

where C is either P for the particle or W for the walls. Eq. (11) may thus be written as

$$\mathbf{u}^D(\mathbf{x}_0)=-\frac{1}{4\pi\mu}[\mathcal{S}(\mathbf{x}_0,\mathbf{f}^D,P)+\mathcal{S}(\mathbf{x}_0,\mathbf{f}^D,W)]+\frac{1}{4\pi}[\mathcal{D}(\mathbf{x}_0,\mathbf{u}^D,P)+\mathcal{D}(\mathbf{x}_0,\mathbf{u}^D,W)]. \tag{14}$$

We substitute $\mathbf{u}^D=\mathbf{u}-\mathbf{u}^\infty=\mathbf{u}^B+\mathbf{u}^S-\mathbf{u}^\infty$ for the particle surface into the third term on the right-hand side of (14), and then apply the reciprocal identity for the background flow over the particle volume and the integral identities for the term expressing rigid-body motion [17]. The integral representation (14) then becomes

$$\mathbf{u}^D(\mathbf{x}_0)=-\frac{1}{4\pi\mu}[\mathcal{S}(\mathbf{x}_0,\mathbf{f},P)+\mathcal{S}(\mathbf{x}_0,\mathbf{f}^D,W)]+\frac{1}{4\pi}[\mathcal{D}(\mathbf{x}_0,\mathbf{u}^S,P)+\mathcal{D}(\mathbf{x}_0,\mathbf{u}^D,W)], \tag{15}$$

which involves the total traction and the slip velocity over the particle surface. Note that on the walls, the disturbance velocity is

$$\mathbf{u}^D=\mathbf{u}^S-\mathbf{u}^\infty=\frac{\varepsilon\zeta_w}{\mu}(\mathbf{I}-\mathbf{nn})\cdot\nabla\phi^D, \tag{16}$$

where $\mathbf{u}^S$ is the total slip velocity due to both the background potential and the disturbance potential.

Apply the boundary integral formulation (14) at a point, $\mathbf{x}_0$, on the particle surface, and use again the integral identity for the particle volume and that for the rigid-body motion, then we derive the integral equation

$$\mathbf{u}^B(\mathbf{x}_0)+\frac{1}{2}\mathbf{u}^S(\mathbf{x}_0)-\mathbf{u}^\infty=-\frac{1}{4\pi\mu}[\mathcal{S}(\mathbf{x}_0,\mathbf{f},P)+\mathcal{S}(\mathbf{x}_0,\mathbf{f}^D,W)]+\frac{1}{4\pi}[\mathcal{D}(\mathbf{x}_0,\mathbf{u}^S,P)+\mathcal{D}(\mathbf{x}_0,\mathbf{u}^D,W)]. \tag{17}$$

Apply (14) at a point, $\mathbf{x}_0$, on the channel walls, and use the integral identities, then we have

$$\frac{1}{2}\mathbf{u}^D(\mathbf{x}_0)=-\frac{1}{4\pi\mu}[\mathcal{S}(\mathbf{x}_0,\mathbf{f},P)+\mathcal{S}(\mathbf{x}_0,\mathbf{f}^D,W)]+\frac{1}{4\pi}[\mathcal{D}(\mathbf{x}_0,\mathbf{u}^S,P)+\mathcal{D}(\mathbf{x}_0,\mathbf{u}^D,W)]. \tag{18}$$

To solve the integral equations (9), (17), and (18), the wall and particle contours are discretized by a non-uniform mesh consisting of linear or arc segments. The unknown variables, ϕ^D on both P and W, $\mathbf{f}$ on P, and $\mathbf{f}^D$ on W, are defined at the element centers. The integral equation for the disturbance potential, (9), is solved first. Then, the slip velocity at the particle surface and walls, $\mathbf{u}^S$, is calculated from Eq. (3), and the disturbance velocity at the walls, $\mathbf{u}^D$, is obtained by subtracting the background velocity according to Eq. (16). Finally, (17) and (18) are solved together with the unknown translational and rotational velocities of the particle. To match the total number of unknowns, two additional equations from (5) expressing vanishing condition of the total traction in x and the total torque on the particle are appended to the linear algebraic system. In all the equations, the integrals are carried out using the Gauss–Legendre quadratures over each element. The singularities of the singular elements are subtracted off and computed analytically. It should be pointed out the current boundary element solver is based on a free online library, BEMLIB [16].

Calculation of the slip velocity in (3) requires evaluation of the tangential derivative of the electric potential. To do this, we compute ϕ at the two end nodes of each element after solving (9) and then approximate the tangential derivative of ϕ at the element center using a second-order finite-difference scheme. The channel is truncated at $x=\pm L/2$ with the particle located at $x=0$. We have chosen $L=30a$ for all simulations. One difficulty arises as the channel width approaches to the particle size, as an exceedingly long domain is needed for $\mathbf{u}^D$ to decay to an acceptable limit. To deal with the problem, we require that the flow be unidirectional at the channel inlet/outlet. Consequently, u_y and f_x are zero at the inlet/outlet, but u_x and f_y are unknown. These additional variables are solved together with the integral equations by including the inlet and outlet in the integration contours. We point out that the non-zero disturbance velocity at the inlet and outlet still satisfies the boundary condition at the walls, Eq. (16). That is, $\mathbf{u}^D$ is zero at the four corners of the channel since the disturbance potential and its gradient vanish at those locations.

4. Results and discussions

In order to validate the accuracy of the present BEM code, we first consider electrophoretic mobility of a cylindrical particle in a semi-infinite flow driven by electroosmosis, that is, the uniform flow due to a non-zero charge on the *single* wall. The analytical solution of this two-dimensional problem was reported by Keh et al. [11]. Fig. 2 plots the normalized translational and rotational velocities of the cylinder, $\hat{U}_p=U_p\mu/\varepsilon(\zeta_p-\zeta_w)E^\infty$, and

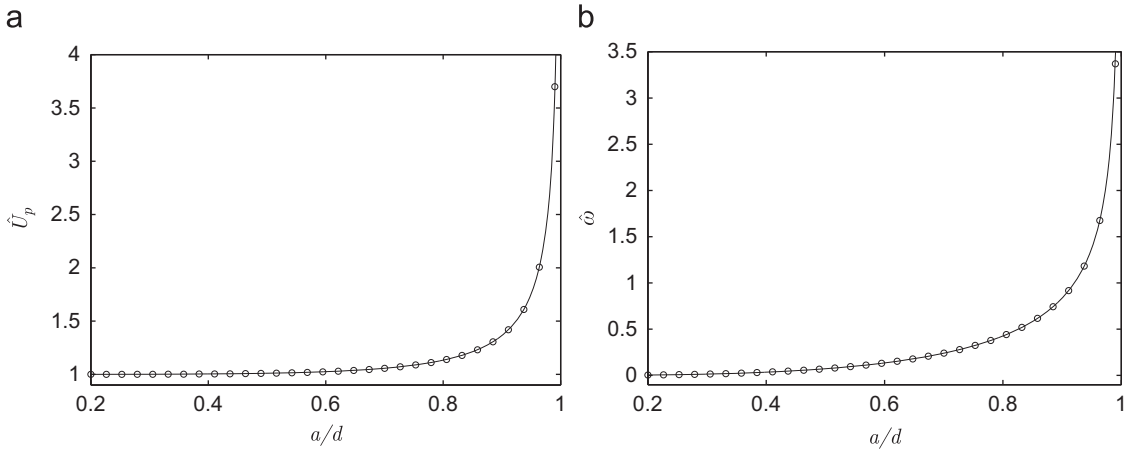

Fig. 2. The normalized (a) translational and (b) rotational velocities of the cylinder as functions of a/d computed from Keh et al. [11] (solid line) and the BEM used in the current study (markers).

Table 1
Comparison of the normalized translational and rotational velocities of the cylinder as functions of a/d computed from Keh et al. [11] and the BEM used in the current study.

a/d	Current study		Keh et al. [11]	
	$\hat{U}_p$	$\hat{\omega}$	$\hat{U}_p$	$\hat{\omega}$
0.20	1.0000	0.0041	1.0002	0.0041
0.60	1.0244	0.1351	1.0250	0.1350
0.80	1.1328	0.4267	1.1333	0.4267
0.90	1.3648	0.8360	1.3650	0.8362
0.95	1.7577	1.3720	1.7574	1.3729
0.98	2.6120	2.3620	2.6121	2.3648
0.99	3.5963	3.4464	3.6149	3.4391

$\hat{\omega}=\omega\mu a/\varepsilon(\zeta_p-\zeta_w)E^{\infty}$, where U_p and ω are the corresponding dimensional quantities in the laboratory coordinates. The results are depicted as functions of the ratio between the particle radius and the distance from the particle center to the lower wall, a/d. It can be seen that the present numerical results are in excellent agreement with the theoretical prediction. The smallest particle–wall separation in the figure is $0.01a$, i.e., $a/d\approx 0.99$, for which we used 256 uniform elements on the particle and 192 non-uniform elements on the wall. The comparison of the numerical calculation with the analytical result for a few selected cases is also provided in Table 1, where the difference is up to the second decimal point for the closest proximity.

When the particle is far away from the wall, the translational velocity approaches the value corresponding to the electrophoretic velocity of the particle in an infinite flow, $\varepsilon(\zeta_p-\zeta_w)E^{\infty}/\mu$, and the rotational velocity approaches zero, as expected. As the particle comes nearly in contact with the wall, both the translational and rotational velocities grow to infinity, which is in sharp contrast with a purely hydrodynamic flow where the particle velocity is reduced by the wall due to viscous retardation. A similar enhancing effect of the wall on the electrophoretic mobility of a nearby spherical particle was reported in Keh and Chen [3] and Yariv and Brenner [5]. As pointed out by them, the phenomenon is caused by the intensified electric field in the narrow gap, which is dominant over the viscous effect and introduces a high slip between the particle and the fluid in the gap.

Next, we consider a particle bounded by two walls. Fig. 3(a,b) shows the particle's translational and rotational velocities at varying distances between the two walls at four reduced channel widths, H/a. As in other two- and three-dimensional particle/channel configurations (e.g., [3–5,11]) where the EDL is assumed to be thin, we also found that U_p and ω are proportional to the difference between the zeta potentials on the particle and wall, $\zeta_p-\zeta_w$. Therefore, the same normalizations for U_p and ω as in the single wall case are used here. To better display the results, the eccentric position of the particle has been scaled by $H-2a$.

For wide channels such as $H/a=20$, the reduced translational velocity and rotational velocity are nearly unity and zero, respectively, for a wide range of particle locations. This reflects the situation of infinite flow and means that the wall effect is negligible. When the particle approaches either one of the two walls, the particle behaves as it would if it were brought within close proximity of only a single wall and the effect of the other wall is negligible.

At smaller values of H/a, the effect of both channel walls on the particle motion becomes evident. When the particle is located away from the walls, its translational velocity is lower compared to the wide channel case, while its rotational velocity is higher. As the particle approaches either wall, both the translational and rotational velocities increase monotonically. The closest particle-wall distance here is 1% of the particle radius. Due to the deteriorated numerical accuracy, we were unable to verify if the particle's velocities would go to infinity when the particle further approaches the wall.

To see how the channel width affects the particle motion at the symmetric configuration, in Fig. 3(c) we plot the reduced velocity against $H/(2a)$ for the particle located at the centerline of the channel. The graph shows that, as the channel approaches the same size of the particle, the translational velocity approaches a value which is around 53% of the unbounded case. This behavior is in contrast with that of the corresponding spherical particle traveling along the centerline of the channel. According to the analytical result of Unni et al. [12], the normalized translational velocity of the sphere decreases slightly as $H/(2a)$ goes from infinity down to around 1.25, and then it starts to increase instead as $H/(2a)$ is further reduced. The translation grows by around 70% when $H/(2a)$ approaches unity.

The reduced mobility of the cylindrical particle in a narrow channel can be understood from the opposing effects of the electrophoresis and viscosity. For a wide channel relative to the particle size, the particle motion induces little friction anywhere between the fluid and the channel walls except within the gap regions, and the mass flow caused by the particle translation can be easily offset by the reversal flow through at least one of the two

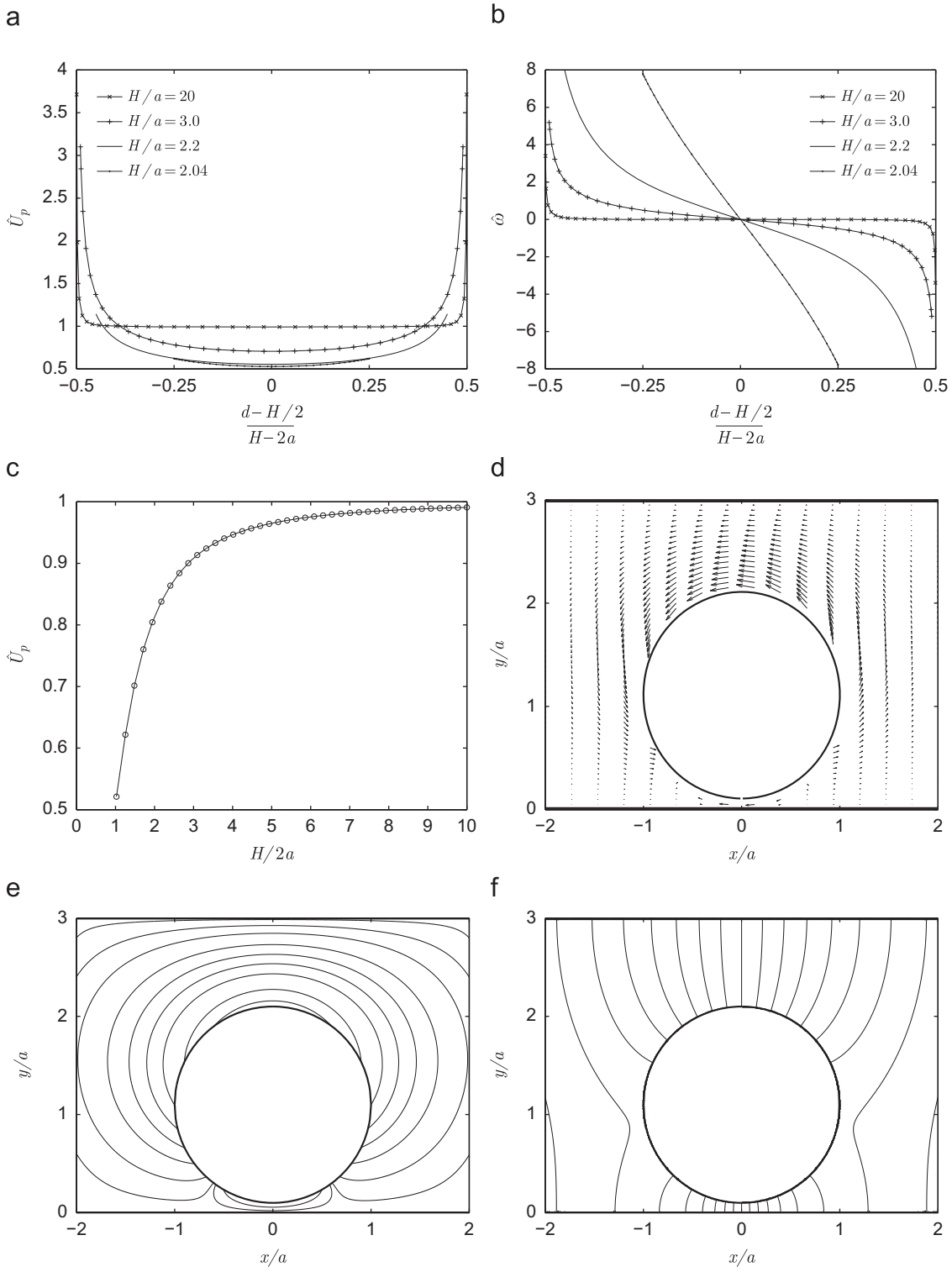

Fig. 3. The translation (a) and rotation (b) of the particle as functions of the normalized eccentricity. (c) The translation of the particle located at the centerline of the channel as a function of H/a. (d) The flow field (the particle is moving from left to right and rotating counterclockwisely), (e) streamline plot and (f) equipotential lines for $H/a=3$, $d/a=1.1$, and $\zeta_w=0$.

particle–wall gaps. Therefore, if the particle is close to either of the walls in a wide channel, the intensified electric field in the smaller gap dominates over the viscous resistance, and as a result, the particle translation is enhanced. When the channel becomes narrow and its width comparable to the particle diameter, due to the friction in the small gaps on both sides of the particle, the amount of the reversal flow is restricted. The particle's translation tends to induce a net flow in the channel due to the mass conservation, but the net flow is subject to the friction between the fluid and entire channel. The narrower the channel is, the stronger the frictional effect becomes. For a particle near the centerline of the channel, the frictional resistance is of the same order as the electric force. Therefore, the particle velocity approaches a limiting value as shown in Fig. 3(c). This "piston

effect" is similar to the spherical particle in a cylindrical pore analyzed in Keh and Chiou [18] and Yariv and Brenner [4], where they found that the particle also approaches a finite velocity as the diameter of the pore becomes increasingly close to that of the particle. In comparison, for a spherical particle in the channel with infinite span, flow can go around the particle easily even when the particle is tightly bounded by the walls. As a result, the electrical force outgrows the hydrodynamic retardation, and the sphere's mobility is enhanced due to the comprehensive wall effect, as shown in Unni et al. [12].

Note that even though the particle's translation is reduced when the channel becomes narrower, its rotation is not. The rotation is caused by the necessary slip velocity on the particle surface as dictated by Eq. (3). Fig. 3(b) shows that $\hat{\omega}$ is zero for a symmetrical configuration, but it grows quickly as soon as the particle is located off the centerline. For smaller H/a, $\hat{\omega}$ can be much larger than 1. Therefore, the particle's rotation is sensitive to its eccentricity in a narrow channel. This increased rotational sensitivity is also observed in Unni et al. [12] for the wall-bounded spherical particle, where, however, $\hat{\omega}$ of the sphere is below unity at least when $H/(2a)$ is above 0.99.

The flow field is visualized in Fig. 3(d) for $H/a=3$ and $d/a=1.1$. The zeta potential on the wall is chosen to be zero so that the electrically neutral walls yield no background velocity and the velocity vectors represent the disturbance velocity from the presence of the particle as computed from Eq. (15). The slip velocity on the particle surface is evident in the figure. In addition, Fig. 3(e) and (f) visualizes streamlines and the contours of the total potential around the particle. In (e), two stagnation points can be seen on the particle's boundary in the region near the lower wall. In (f), the potential undergoes a quick change along the narrower gap between the particle and channel, causing a high slip velocity of the fluid on both the particle surface and wall in the region.

5. Conclusion

We have adopted a boundary-element method to solve for the electrophoretic mobility of a cylindrical particle placed in a rectangular channel with arbitrary eccentricity. Both the particle and walls are non-conducting, and the electrical double layers adjacent to the solid surfaces are assumed to be thin with respect to the particle radius and to the particle–wall gap. When the ratio between the channel width and cylinder diameter approaches unity, the viscous effect becomes comparable to the electrophoresis and the translational velocity of the particle reaches a finite value determined by the eccentricity. In addition, the rotational velocity of a closely fitting particle is sensitive to its eccentricity.

Acknowledgments

The present solver is heavily based on the BEMLIB, a free online software library developed by Professor C. Pozrikidis of University of Massachusetts, Amherst, whose effort is gratefully acknowledged.

References

[1] Stone HA, Stroock AD, Ajdari A. Engineering flows in small devices: microfluidics toward a lab-on-a-chip. Annu Rev Fluid Mech 2004;36:381–411.
[2] Keh HJ, Anderson JL. Boundary effects on electrophoretic motion of colloidal spheres. J Fluid Mech 1985;153:417–39.
[3] Keh HJ, Chen SB. Electrophoresis of a colloidal sphere parallel to a dielectric plane. J Fluid Mech 1988;194:377–90.
[4] Yariv E, Brenner H. The electrophoretic mobility of a closely fitting sphere in a cylindrical pore. SIAM J Appl Math 2003;64(2):423–41.
[5] Yariv E, Brenner H. Near-contact electrophoretic motion of a sphere parallel to a planar wall. J Fluid Mech 2003;484:85–111.
[6] Hsu JP, Kuo CC. Electrophoresis of a finite cylinder positioned eccentrically along the axis of a long cylindrical pore. J Phys Chem B 2006;110(35):17607–15.
[7] Hsu JP, Chen ZS, Ku MH, Yeh LH. Effect of charged boundary on electrophoresis: sphere in spherical cavity at arbitrary potential and double-layer thickness. J Colloid Interface Sci 2007;314(1):256–63.
[8] Keh HJ, Hsieh TH. Electrophoresis of a colloidal sphere in a spherical cavity with arbitrary zeta potential distributions and arbitrary double-layer thickness. Langmuir 2008;24(2):390–8.
[9] Ye C, Li D. 3-D transient electrophoretic motion of a spherical particle in a T-shaped rectangular microchannel. J Colloid Interface Sci 2004;272(2):480–8.
[10] Davison SM, Sharp KV. Transient simulations of the electrophoretic motion of a cylindrical particle through a 90 degrees corner. Microfluid Nanofluidics 2008;4(5):409–18.
[11] Keh HJ, Horng KD, Kuo J. Boundary effects on electrophoresis of colloidal cylinders. J Fluid Mech 1991;231:211–28.
[12] Unni HN, Keh HJ, Yang C. Analysis of electrokinetic transport of a spherical particle in a microchannel. Electrophoresis 2007;28(4):658–64.
[13] O'Brien RW. The solution of the electrokinetic equations for colloidal particles with thin double layers. J Colloid Interface Sci 1983;92:204–16.
[14] Sellier A. On boundary effects in electrophoresis. C R Acad Sci Ser IIb 2001;329(8):565–70.
[15] Allison SA, Xin Y. Electrokinetic transport of rigid macroions in the thin double layer limit: a boundary element approach. J Colloid Interface Sci 2005;288(2):616–28.
[16] Pozrikidis C. A practical guide to boundary element methods with the software library BEMLIB. Boca Raton, FL: CRC Press; 2002.
[17] Pozrikidis C. Boundary integral and singularity methods for linearized viscous flow. New York: Cambridge University Press; 1992.
[18] Keh HJ, Chiou JY. Electrophoresis of a colloidal sphere in a circular cylindrical pore. AIChE J 1996;42(5):1397–406.